

Extraction of Propagation Delay-Correlated Mobility and Its Verification for Amorphous InGaZnO Thin-Film Transistor-Based Inverters

Kyung Min Lee, Jaeman Jang, Sung-Jin Choi, Dong Myong Kim, *Member, IEEE*,
Kyung Rok Kim, *Member, IEEE*, and Dae Hwan Kim, *Senior Member, IEEE*

Abstract—We found that field-effect mobility, which had been widely used in the evaluation of the mobility of an amorphous indium–gallium–zinc oxide (a-IGZO) thin-film transistor (TFT) failed to describe the effect of mobility on propagation delay (t_{PD}) in an a-IGZO TFT-based circuit, and also proposed an extraction technique for the t_{PD} -correlated mobility ($\mu_{t_{PD}}$) considering both the subgap density-of-states and the voltage-dependent charge density. It is verified that the proposed $\mu_{t_{PD}}$ is the best correlated with the measured t_{PD} in IGZO TFT-based inverters other than various mobilities in the literature. Our results have revealed that it is possible to predict t_{PD} only with the measured current–voltage characteristic of the a-IGZO TFT without measuring t_{PD} in IGZO-based circuits.

Index Terms—Amorphous indium–gallium–zinc oxide (a-IGZO), mobility, propagation delay, subgap density-of-states (DOSs), thin-film transistors (TFTs).

I. INTRODUCTION

AMORPHOUS indium–gallium–zinc oxide (a-IGZO) has been a representative and promising material as an active layer of thin-film transistor (TFT) for potential applications in oxide-semiconductor-based high-frame-rate large-area displays, flexible, transparent, mobile displays, and logic/memory circuitry, because it has a high carrier mobility, large-area uniformity, good transparency in visible light, a low OFF-current, cost-effectiveness of the fabrication process, and compatibility with a low-temperature process as well a solution process [1]–[3]. In real applications, the circuit performance is influenced mainly by the carrier mobility of the TFT as long as there is either a maintaining operating voltage or a load capacitance. Therefore, most of the material- or fabrication-aspect studies have primarily

Manuscript received May 21, 2014; accepted March 11, 2015. Date of publication March 25, 2015; date of current version April 20, 2015. This work was supported in part by the National Research Foundation of Korea through the Korea Government within the Ministry of Science, ICT and Future Planning under Grant 2013065339, in part by the BK21+ Educational Research Team for Creative Engineers on Material-Device-Circuit Co-Design under Grant 22A2013000042, in part by the Year of 2014 UNIST Research Fund, and in part by the IC Design Education Center. The review of this paper was arranged by Editor K. C. Choi. (*Corresponding author: Kyung Rok Kim and Dae Hwan Kim.*)

K. M. Lee, J. Jang, S.-J. Choi, D. M. Kim, and D. H. Kim are with the School of Electrical Engineering, Kookmin University, Seoul 136-702, Korea (e-mail: drlife@kookmin.ac.kr).

K. R. Kim is with the School of Electrical and Computer Engineering, Ulsan National Institute of Science and Technology, Ulsan 689-798, Korea (e-mail: krkim@unist.ac.kr).

Color versions of one or more of the figures in this paper are available online at <http://ieeexplore.ieee.org>.

Digital Object Identifier 10.1109/TED.2015.2413941

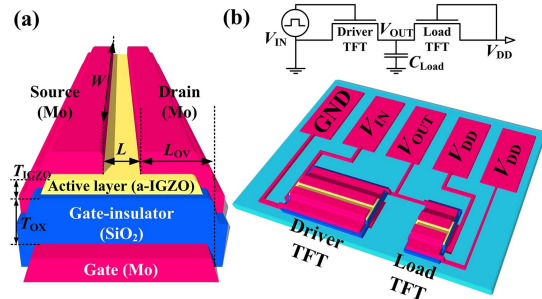


Fig. 1. Schematics of (a) a-IGZO TFT with the inverted staggered bottom-gate structure and (b) enhancement load-type a-IGZO TFT-based inverter.

contributed to improving the carrier mobility with the belief that the propagation delay (t_{PD}) of circuits is inversely proportional to the carrier mobility. However, field-effect mobility (μ_{FE}), which is widely used as the practically extracted carrier mobility, has seldom been correlated with the t_{PD} measured in a-IGZO TFT-based circuits. The mobility-based assessment for circuit performance would evoke a huge error unless the extracted mobility is inversely proportional to a real t_{PD} , which is the main motive of our work.

In this paper, we propose a practical method for extracting the circuit propagation delay-correlated mobility ($\mu_{t_{PD}}$) from electrical characteristics of a-IGZO TFTs with the detailed procedure of parameter extracting. It was found the $\mu_{t_{PD}}$, the backbone of which originated from the charge-based mobility, is best correlated with the measured t_{PD} other than various mobilities that have been in the literature, such as μ_{FE} and the average mobility (μ_{avg}). In comparison with μ_{FE} and μ_{avg} , our results reveal that such a good correlation of $\mu_{t_{PD}}$ with t_{PD} is ascribed to two reasons. First, the density-of-states (DOSs) and the carrier density, the latter of which is modulated by the gate voltage, are considered in extracting $\mu_{t_{PD}}$. The other reason is that the subthreshold and above-threshold characteristics, which are essentially important in the operation of IGZO TFT-based circuitry, can be befittingly combined with each other.

II. INVERTER INTEGRATION

Three inverters with individually different geometries and fabrication processes were integrated on glass wafers. They were based on a-IGZO TFTs with inverted staggered bottom-gate structures, as shown in Fig. 1(a). The enhancement load-type inverter consists of two a-IGZO TFTs, as shown in Fig. 1(b).

TABLE I
CHARACTERISTIC PARAMETERS AND SYMBOLS

Common parameter	Symbol	Value	Unit
Dielectric constant of a-IGZO	ϵ_{IGZO}	11.5	
Bulk-Fermi potential	ϕ_{F0}	0.3	V
Gate-to-S/D overlap length	L_{OV}	10	μm
Thickness of gate insulator	T_{OX}	100	nm
Sample A parameter	Symbol	Value	Unit
Width for the driver TFT	W_{Driver}	270	μm
Width for the load TFT	W_{Load}	70	μm
Length for the driver/load TFT	L	10	μm
Thickness of a-IGZO thin film	T_{IGZO}	40	nm
Oxide capacitance	C_{OX}	37.4	nF/cm ²
Conduction band mobility	μ_{Band}	13.2	cm ² /V·s
Effective DOS in conduction band	N_C	2.5×10^{18}	$\mu\text{F}/\text{cm}^2$
Threshold voltage	V_T	-1.98	V
Flat band voltage	V_{FB}	-2.61	V
Effective charge density (sub- V_T)	N_{eff1}	1.94×10^{18}	cm ⁻³
Effective characteristic energy (sub- V_T)	kT_{eff1}	0.0412	eV
Effective charge density (above- V_T)	N_{eff2}	2.54×10^{18}	cm ⁻³
Effective characteristic energy (above- V_T)	kT_{eff2}	0.0260	eV
Sample B parameter	Symbol	Value	Unit
Width for driver TFT	W_{Driver}	250	μm
Width for load TFT	W_{Load}	50	μm
Length for the driver/load TFT	L	30	μm
Thickness of a-IGZO thin film	T_{IGZO}	50	nm
Gate oxide capacitance per unit area	C_{OX}	43.07	nF/cm ²
Conduction band mobility	μ_{Band}	14.8	cm ² /V·s
Effective DOS in conduction band	N_C	4×10^{18}	$\mu\text{F}/\text{cm}^2$
Threshold voltage	V_T	0.82	V
Flat band voltage	V_{FB}	-1.20	V
Effective charge density (sub- V_T)	N_{eff1}	1.79×10^{18}	cm ⁻³
Effective characteristic energy (sub- V_T)	kT_{eff1}	0.0655	eV
Effective charge density (above- V_T)	N_{eff2}	6.19×10^{18}	cm ⁻³
Effective characteristic energy (above- V_T)	kT_{eff2}	0.0323	eV
Sample C parameter	Symbol	Value	Unit
Width for driver TFT	W_{Driver}	250	μm
Width for load TFT	W_{Load}	50	μm
Length for the driver/load TFT	L	5	μm
Thickness of a-IGZO thin film	T_{IGZO}	50	nm
Oxide capacitance	C_{OX}	34.53	nF/cm ²
Conduction band mobility	μ_{Band}	16.6	cm ² /V·s
Effective DOS in conduction band	N_C	4.81×10^{18}	$\mu\text{F}/\text{cm}^2$
Threshold voltage	V_T	-1.70	V
Flat band voltage	V_{FB}	-3.45	V
Effective charge density (sub- V_T)	N_{eff1}	1.50×10^{18}	cm ⁻³
Effective characteristic energy (sub- V_T)	kT_{eff1}	0.0630	eV
Effective charge density (above- V_T)	N_{eff2}	6.40×10^{18}	cm ⁻³
Effective characteristic energy (above- V_T)	kT_{eff2}	0.0295	eV

The details of the fabrication process, such as the cation composition, the condition of gate insulator deposition, and the degree of oxygen deficiency of IGZO, were different from one another among three inverters, although their standard fabrication procedures were consistent with those discussed in [4]. The influence of the process on the device characteristic was fully reflected into our study using process-controlled parameters shown in Table I. Three inverters (Sample A, B, and C) made it possible to compare the measured t_{PD} with the variations of both the TFT mobility and the load capacitance.

The geometrical parameters were summarized in Table I. The gate-to-source/drain overlap length (L_{OV}) and the thickness of gate oxide insulator (T_{OX}) are the same with

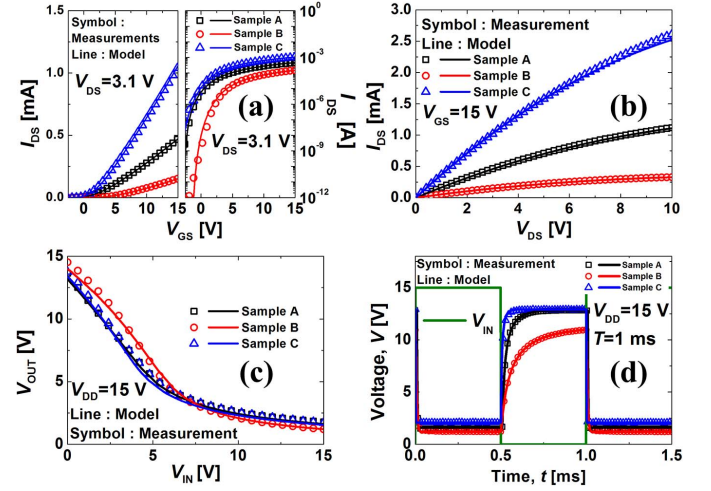


Fig. 2. Measured (a) I_{DS} - V_{GS} characteristics at $V_{DS} = 3.1$ V and (b) I_{DS} - V_{DS} characteristics at $V_{GS} = 15$ V in driver TFTs. (c) V_{IN} - V_{OUT} VTCs at $V_{DD} = 15$ V. (d) V_{IN} - V_{OUT} transient responses at $V_{IN} = 0 \sim 15$ V with $T = 1$ ms, $t_r = 1 \mu\text{s}$, $t_f = 1 \mu\text{s}$, and duty = 50%, which were measured in IGZO inverters. For all the figures, the lines are the calculated ones using the model in [4].

one another, i.e., $L_{OV} = 10 \mu\text{m}$ and $T_{OX} = 100$ nm. The channel length (L), the channel width of load/driver TFT (W_{Load}/W_{Driver}), the thickness of a-IGZO thin-film (T_{IGZO}), and the threshold voltage (V_T) are as follows: 1) $L = 10 \mu\text{m}$, $W_{Load}/W_{Driver} = 70/270 \mu\text{m}$, $T_{IGZO} = 40$ nm, and $V_T = -1.98$ V (Sample A); 2) $L = 30 \mu\text{m}$, $W_{Load}/W_{Driver} = 50/250 \mu\text{m}$, $T_{IGZO} = 50$ nm, and $V_T = 0.82$ V (Sample B); and 3) $L = 5 \mu\text{m}$, $W_{Load}/W_{Driver} = 50/250 \mu\text{m}$, $T_{IGZO} = 50$ nm, and $V_T = -1.70$ V (Sample C), respectively.

The transfer characteristic of the drain-to-source dc current (I_{DS}) versus gate-to-source voltage (V_{GS}) [symbol in Fig. 2(a)] and the output characteristic of the I_{DS} versus drain-to-source voltage (V_{DS}) [symbol in Fig. 2(b)] were measured in IGZO driver TFTs. The voltage transfer curves (VTCs) [symbol in Fig. 2(c)] were also measured in IGZO inverters using the Agilent 4156C semiconductor parameter analyzer. Transient response of the output voltage of an inverter was measured with the oscilloscope [symbol in Fig. 2(d)]. The capacitance-voltage (C - V) characteristics were measured using Agilent 4294A precision impedance analyzer (not shown here). All measurements were performed at room temperature and under a dark ambient condition. The output voltage of inverter (V_{OUT}) was toggled between the maximum (V_{MAX}) and the minimum value of V_{OUT} (V_{MIN}) when the input voltage of inverter (V_{IN}) was toggled between 0 and 15 V with the period (T) = 1 ms, the rising and falling time (t_r and t_f) = 1 μs , duty = 50%, and the power supply voltage $V_{DD} = 15$ V. Then, the V_{MAX}/V_{MIN} was measured to be 12.82/1.51 V (Sample A), 10.98/1.18 V (Sample B), and 12.91/2.09 V (Sample C), respectively. In addition, the average output voltage V_{MID} was defined as $V_{MID} = (V_{MAX} + V_{MIN})/2$ and the t_{PD} was measured with the definition of $t_{PD} = (t_{PHL} + t_{PLH})/2$, where the t_{PHL} (t_{PLH}) was the delay time during the transition between V_{MAX} (V_{MIN}) and V_{MID} . Finally, the measured t_{PD} was 8.07 μs (Sample A), 24.14 μs (Sample B),

TABLE II
EXTRACTED MOBILITIES AND MEASURED t_{PD} s TAKEN
FROM THREE KINDS OF INVERTERS

Sample ID	μ_{PD} [cm ² /Vs]	μ_{FE} [cm ² /Vs]	μ_{avg} [cm ² /Vs]	$V_{MID}/V_{MAX}/$ V_{MIN} [V]
Sample A	9.80	13.2	8.95	7.17 / 12.82 / 1.51
Sample B	10.08	14.8	9.54	6.08 / 10.98 / 1.18
Sample C	12.30	16.6	9.58	7.50 / 12.91 / 2.09

Sample ID	C_{Load} [pF]	t_{PHL} [μs]	t_{PLH} [μs]	t_{PD} [μs]
Sample A	323	1.95	14.19	8.07
Sample B	295	5.61	42.67	24.14
Sample C	217	0.63	4.80	2.71

and 2.71 μs (Sample C), respectively. The measured V_{MID} , V_{MAX} , V_{MIN} , t_{PD} , t_{PHL} , and t_{PLH} of three inverters were abridged in Table II.

III. MOBILITY MODEL

The proposed mobility model is established on the charge-based mobility $\mu_{CB} = \mu_{Band} \times Q_{free}/(Q_{free} + Q_{loc})$ [5], [6] with μ_{Band} = conduction band mobility, Q_{free} = the charge density per unit area by free carriers, and Q_{loc} = the localized charge density per unit area. The $g_A(E)$, i.e., the subgap DOS near the conduction band minimum (E_C), consists of the acceptor-like tail state [$g_{TA}(E)$] and the acceptor-like deep state [$g_{DA}(E)$], and the energy distributions of which can be modeled as follows:

$$\begin{aligned} g_A(E) &= g_{DA}(E) + g_{TA}(E) \\ &= N_{DA} \times \exp\left(\frac{E - E_C}{kT_{DA}}\right) \\ &\quad + N_{TA} \times \exp\left(\frac{E - E_C}{kT_{TA}}\right) \text{ [cm}^{-3}\text{eV}^{-1}\text{]}. \end{aligned} \quad (1)$$

Here, Q_{free} and Q_{loc} can be calculated as

$$\begin{aligned} Q_{free}(x) &= Q_{free}(\phi(x)) = q \int_x^{x=T_{IGZO}} n_{free}(x) dx \\ &= q \int_x^{x=T_{IGZO}} N_C \times \exp\left(\frac{q(\phi(x) - \phi_{F0} - V_{CH})}{kT}\right) dx \end{aligned} \quad (2)$$

$$\begin{aligned} Q_{loc}(x) &= Q_{loc}(\phi(x)) = q \int_x^{x=T_{IGZO}} n_{loc}(x) dx \\ &= q \int_x^{x=T_{IGZO}} \frac{N_{TA} \cdot \pi \cdot kT}{\sin(\pi T/T_{TA})} \exp\left(\frac{q(\phi(x) - \phi_{F0} - V_{CH})}{kT_{TA}}\right) dx \end{aligned} \quad (3)$$

where q is the elementary charge, x is a location along the vertical direction from the a-IGZO/gate insulator interface, n_{free} is the free carrier density, N_C is the effective DOS in conduction band, $\phi(x)$ is the electric potential along the x -direction, ϕ_{F0} is the bulk-Fermi potential, V_{CH} is a channel potential varied along the channel length direction at a fixed V_{DS} (i.e., the potential difference describing the electron quasi-Fermi level E_{Fn} lowered by qV_{CH} due to applied V_{DS}), k is the Boltzmann constant, T is an absolute temperature, and n_{loc} is the localized state density.

The charge density $\rho(x)$ can be approximated as

$$\begin{aligned} \rho(x) &= -q \times N_{eff1} \exp\left(\frac{q(\phi(x) - V_{CH} - \phi_{F0})}{kT_{eff1}}\right), \\ &\quad \text{for } V_{FB} < V_{GS} < V_T \\ \rho(x) &= -q \times N_{eff2} \exp\left(\frac{q(\phi(x) - V_{CH} - \phi_{F0})}{kT_{eff2}}\right), \\ &\quad \text{for } V_{GS} > V_T \end{aligned} \quad (4)$$

where N_{eff1} and kT_{eff1} are the effective state density and effective characteristic energy which are dominated in the subthreshold ($V_{FB} < V_{GS} < V_T$) region with V_{FB} being the flat-band voltage. Then, N_{eff1} and kT_{eff1} can be calculated directly from the DOS parameters [7] as

$$N_{eff1} = \frac{N_{TA} \cdot \pi \cdot kT}{\sin(\pi T/T_{TA})}, \quad kT_{eff1} = kT_{TA} \quad (5)$$

because a total charge in the subthreshold region is dominated by the charge localized in $g_{TA}(E)$. On the other hand, N_{eff2} and kT_{eff2} are the effective state density and effective characteristic energy which are dominated in the above-threshold ($V_{GS} > V_T$) condition. They can be extracted from fitting the measured current-voltage (I - V) curves with the calculated ones as discussed in Section IV. The effective charge-based mobility $\mu_{eff} = \mu_{Band} \times Q_{free}/(Q_{free} + Q_{loc})$ can be then derived as [4]

$$\begin{aligned} \mu_{eff}(\phi(x)) &= \mu_{eff}(N_{effi}, kT_{effi}) = \mu_{Band} \times \frac{Q_{free}(\phi(x))}{\epsilon_{IGZO} E_{IGZO}(\phi(x))} \\ &= \mu_{Band} \times \frac{A_i^* \times \exp[B_i^* q(\phi(x) - \phi_{F0} - V_{CH})]}{B_i^* \times \sqrt{2\epsilon_{IGZO} N_{effi} kT_{effi}} \times \exp\left(\frac{q(\phi(x) - \phi_{F0} - V_{CH})}{2kT_{effi}}\right)} \end{aligned} \quad (6)$$

$$A_i^* \equiv \frac{N_C \sqrt{\epsilon_{IGZO}}}{\sqrt{2N_{effi} kT_{effi}}}, \quad B_i^* \equiv \left(\frac{1}{kT} - \frac{1}{2kT_{effi}}\right), \quad \text{and } i = 1 \text{ or } 2 \quad (7)$$

where ϵ_{IGZO} is the dielectric constant of a-IGZO and E_{IGZO} is the vertical electric field in the a-IGZO film. The lumped μ_{eff} , i.e., μ_{EFF} , can be then modeled with substituting $\phi(x)$ by ϕ_S and replacing V_{CH} by V_{DS} , respectively, as shown in

$$\begin{aligned} \mu_{EFF}(V_{GS}, V_{DS}, N_{effi}, kT_{effi}) &= \mu_{Band} \times \frac{A_i^* \times \exp[B_i^* q(\phi_S - \phi_{F0} - V_{DS})]}{B_i^* \times \sqrt{2\epsilon_{IGZO} N_{effi} kT_{effi}} \times \exp\left(\frac{q(\phi_S - \phi_{F0} - V_{DS})}{2kT_{effi}}\right)} \end{aligned} \quad (8)$$

$$\begin{aligned} V_{GS} &= V_{FB} + \phi_S + \frac{\sqrt{2\epsilon_{IGZO} N_{effi} kT_{effi}}}{C_{OX}} \\ &\quad \times \exp\left[\frac{q(\phi_S - \phi_{F0} - V_{DS})}{2kT_{effi}}\right], \quad i = 1 \text{ or } 2 \end{aligned} \quad (9)$$

where ϕ_S is the surface potential, i.e., $\phi(x = 0)$. Finally, the t_{PD} -correlated mobility μ_{tPD} can be derived by combining the μ_{EFF} in subthreshold region, i.e., $\mu_{EFF}(N_{eff1}, kT_{eff1})$, and the μ_{EFF} in above-threshold

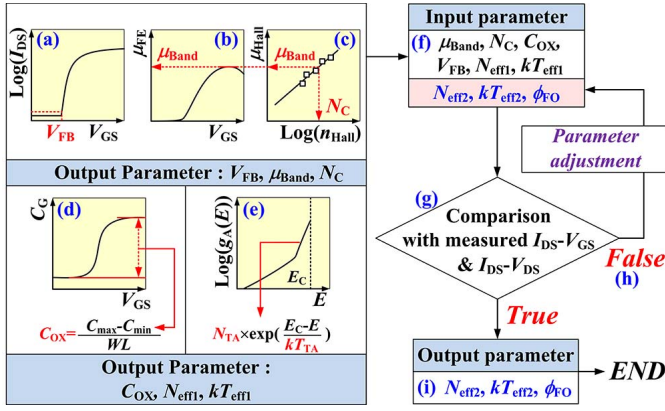


Fig. 3. The procedure of extracting the parameters, such as (a) V_{FB} , (b) μ_{Band} , (c) N_C , (d) C_{OX} , (e) N_{TA} and kT_{TA} (i.e., N_{eff1} and kT_{eff1}), and (f)–(i) N_{eff2} , kT_{eff2} , and ϕ_{FO} .

region, i.e., μ_{EFF} (N_{eff2} , kT_{eff2}) as

$$\mu_{tpD}(V_{GS}, V_{DS}) = [(\mu_{EFF}(V_{GS}, V_{DS}, N_{eff1}, kT_{eff1}))^{-n} + (\mu_{EFF}(V_{GS}, V_{DS}, N_{eff2}, kT_{eff2}))^{-n}]^{-1/n}. \quad (10)$$

In our case, we found that the $n = 1$ is the best way to reproduce the universal relation of $\mu_{tpD} \propto 1/t_{pD}$ for representative kinds of IGZO TFTs (shown in Fig. 5). It suggests that a radical transition of mobility between the subthreshold and above-threshold regions can be contrarily harmful to reproduce either the measured $I-V$ or t_{pD} of IGZO TFTs. It may be because a-IGZO TFT has an inferior ON-OFF switching characteristic to that of a single-crystalline silicon transistor. The n would be practically a fitting parameter that should be modulated according to the device parameters, such as V_{DD} and DOS, as well as the operation temperature.

IV. PARAMETER EXTRACTION

Fig. 3 shows the procedure extracting parameters that are used in calculating the proposed μ_{tpD} (10).

First of all, V_{FB} was extracted as the V_{GS} value where the $I_{DS}(V_{GS})$ prominently rose in the transfer characteristic [Fig. 3(a)], whereas μ_{Band} was set as the maximum value of $\mu_{FE}(V_{GS}) (= g_m(V_{GS})/[C_{OX}(W/L)V_{DS}]$ at $V_{DS} = 0.1$ V [Fig. 3(b)] (the limitation of $\mu_{FE}(V_{GS})$ will be discussed later). The following is the supporting basis for the procedure of determining μ_{Band} . In IGZO TFT, the Fermi energy level E_F gets closer to E_C as V_{GS} increases. Once the E_F goes above the E_C , the carrier mobility begins to be strongly influenced by potential barriers that are randomly distributed around the conduction bandedge [8]–[10]; it would cause degradation of the mobility when E_F rises above the E_C . Therefore, we assumed the condition of the maximum value of measured $\mu_{FE}(V_{GS})$ corresponds to the condition of $E_F(V_{GS}) = E_C$.

On the other hand, in order to determine N_C , we changed the carrier density in thermal equilibrium through modulating the plasma treatment maintaining the other process conditions the same with ones when the IGZO film or TFT was fabricated. Then, the Hall measurement

was carried out to the each carrier density-modulated sample in order to get the relation of Hall mobility versus Hall carrier density, $\mu_{Hall} - n_{Hall}$ [rectangular symbols in Fig. 3(c)]. The value of N_C was then extracted from the value of n_{Hall} corresponding with the condition of $\mu_{Hall}(n_{Hall}) = \mu_{Band}$ [Fig. 3(c)], which is based on the implication that the carrier density would be $n_{free}(V_{GS}) \approx N_C$ when $E_F(V_{GS}) = E_C$ because the electron in IGZO TFTs follows the Fermi–Dirac distribution in nondegenerate semiconductors. Here, it is noteworthy that N_C is a constant determined by the carrier effective mass. However, we should also pay meticulous attention to the relationship between the electron effective mass of IGZO and the fabrication process has not been experimentally and/or systematically analyzed yet. Therefore, we believe that our approximation is practically useful for assessing the process-dependent values of N_C and μ_{Band} .

The gate oxide capacitance per unit area (C_{OX}) was extracted through the measured $C-V$ characteristic between two electrodes, i.e., the gate and the source, which is electrically tied with drain. In specific, the C_{OX} value was extracted as the value of $(C_{max} - C_{min})/WL$, where C_{max} and C_{min} were the maximum and minimum value of the measured $C-V$ characteristic [Fig. 3(d)]. The assumption of $(C_{max} - C_{min}) = W \times L \times C_{OX}$ is very reasonable because C_{max} signifies the conditions in which the channel of TFT gets fully accumulated, whereas C_{min} signifies the channel of TFT being fully depleted [11]. In addition, the $g_A(E)$ was extracted from the measured $C-V$ frequency dependence of a-IGZO TFT [12], and N_{eff1} and kT_{eff1} were determined by (5) using N_{TA} and kT_{TA} from the extracted $g_A(E)$ parameters in (1) [Fig. 3(e)].

The $I_{DS}(V_{GS}, V_{DS})$ can be then calculated through the DOS-based $I-V$ model [4]. Therefore, the N_{eff2} , kT_{eff2} , and ϕ_{FO} were determined by adjusting them as fitting parameters with a numerical iteration until the calculated $I_{DS}(V_{GS}, V_{DS})$ and the measured $I_{DS}(V_{GS}, V_{DS})$ became identical [Fig. 3(f)–(i)]. Finally, the extracted model parameters were summarized in Table I.

Before embarking on ensuring the relationship between t_{pD} and the mobility, the μ_{tpD} and the other mobilities in the literatures, such as μ_{FE} and μ_{avg} , were extracted and compared with one another for each driver TFT in IGZO inverter (Sample A, B, and C) as a function of V_{GS} under the same $V_{DS} = 0.1$ V, as shown in Fig. 4. Here, μ_{FE} was extracted from $\mu_{FE} = g_m/[C_{OX}(W/L) \times V_{DS}]$ and μ_{avg} was determined by Hoffman’s method [13]. μ_{tpD} was extracted from (10) and parameters in Table I. Here, it should be noted in Fig. 4 that the V_{GS} dependence of μ_{tpD} , μ_{FE} , and μ_{avg} are deviated from one another even under the same $V_{DS} = 0.1$ V.

In fact, $\mu_{FE}(V_{GS})$ overestimates the value of mobility because of the inherent limitation that $\mu_{FE} = g_m/[C_{OX}(W/L) \times V_{DS}]$ is based on the assumption μ_{FE} has a constant value, which is independent of V_{GS} . Moreover, μ_{FE} is calculated from the long-channel MOSFET model [14], and inappropriate for IGZO TFTs because it cannot fully reflect the effects of subgap DOS of IGZO upon assessing the TFT mobility. On the other hand, in terms of μ_{avg} , it should

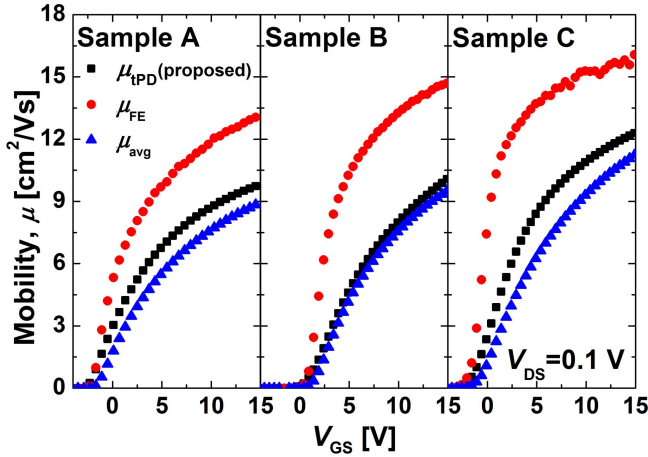


Fig. 4. Experimentally extracted μ_{IPD} , μ_{FE} , and μ_{avg} as a function of V_{GS} with $V_{\text{DS}} = 0.1$ V for driver TFT in a-IGZO inverter.

be highlighted that μ_{avg} is a more appropriate mobility metric for general use in quantifying device performance and a direct, parameter-free assessment of mobility compared with μ_{CB} and μ_{IPD} [13].

Consistently with μ_{avg} , our $\mu_{\text{IPD}}(V_{\text{GS}})$ reflects the V_{GS} dependence of mobility which is excluded in μ_{FE} . Moreover, the proposed $\mu_{\text{IPD}}(V_{\text{GS}})$ includes the effects of subgap DOS on the V_{GS} dependence of mobility as derived from (6)–(10). For the validity of model parameters shown in Table I, it is noteworthy that the calculation results of I – V , VTC, and transient characteristics of the IGZO inverters are well matched with the measured results as denoted by the lines in Fig. 2. Therefore, it can be said that the used parameters and extraction method are reasonably established and can precisely describe the characteristics of three inverters. Noticeably, $\mu_{\text{IPD}}(V_{\text{GS}})$ provides the physical validity as well as practical usefulness, which would be verified in Section V by scrutinizing the relation between μ_{IPD} and the measured t_{PD} of a-IGZO TFT-based inverters.

V. RESULTS AND DISCUSSION

In order to compare the μ_{IPD} , μ_{FE} , and μ_{avg} one another in terms of the universal relation of $\mu \propto 1/t_{\text{PD}}$, we correlated the measured t_{PD} to $1/\mu$ as follows.

Based on the assumption that both V_{DD} and C_{Load} are the same, the measured t_{PD} would be inversely proportional to the extracted mobility. The t_{PD} of sample j ($j = \text{A, B, or C}$), i.e., $t_{\text{PD},j}$, was normalized to the t_{PD} of a referential sample, i.e., $t_{\text{PD,ref}}$, in order to consider only the μ -dependence of t_{PD} , since the three inverters have different values of C_{OX} , C_{Load} , V_{MID} , V_{T} , and W/L . If the C_{OX} , C_{Load} , V_{MID} , V_{T} , and W/L of sample j are defined as $C_{\text{OX},j}$, $C_{\text{Load},j}$, $V_{\text{MID},j}$, $V_{\text{T},j}$, and $(W/L)_j$, respectively, and the C_{OX} , C_{Load} , V_{MID} , V_{T} , and W/L of a referential sample are individually defined as $C_{\text{OX,ref}}$, $C_{\text{Load,ref}}$, $V_{\text{MID,ref}}$, $V_{\text{T,ref}}$, and $(W/L)_{\text{ref}}$, the normalized t_{PD} of sample j ($t_{\text{PD,nor},j}$) can be calculated as

$$t_{\text{PD,nor},j} = t_{\text{PD,ref}} \times \frac{C_{\text{Load,ref}}}{C_{\text{Load},j}} \times \frac{V_{\text{MID,ref}}}{V_{\text{MID},j}} \times \frac{C_{\text{OX},j}}{C_{\text{OX,ref}}}, \quad \text{and } j = \text{A, B, and C.}$$

$$\times \frac{(W/L)_j}{(W/L)_{\text{ref}}} \times \frac{(V_{\text{DD}} - V_{\text{T},j})^2}{(V_{\text{DD}} - V_{\text{T,ref}})^2}. \quad (11)$$

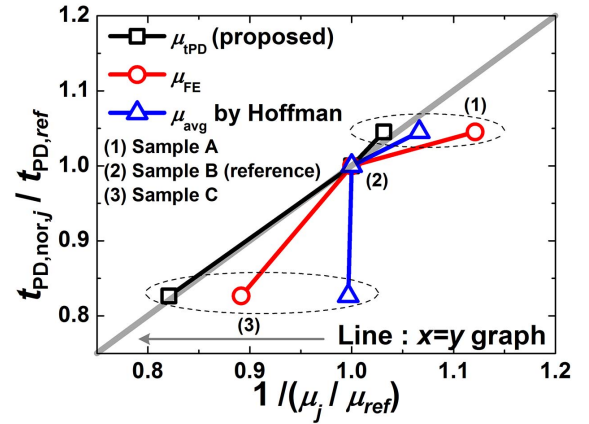


Fig. 5. Plot of $t_{\text{PD,nor},j}/t_{\text{PD,ref}}$ versus $1/(\mu_j/\mu_{\text{ref}})$ for each sample using three different mobilities.

Then, after correcting the sample-to-sample differences of C_{OX} , C_{Load} , V_{MID} , V_{T} , and W/L , i.e., by employing $t_{\text{PD,nor},j}$, the relation of $t_{\text{PD,nor},j}/t_{\text{PD,ref}} = 1/(\mu_j/\mu_{\text{ref}})$ should be satisfied if and only if the mobility of sample j (μ_j) is inversely proportional to the t_{PD} of sample j ($t_{\text{PD},j}$). Here, μ_{ref} is the mobility of a referential sample and the $t_{\text{PD,nor},j}$ when $j = \text{ref}$ specifically becomes $t_{\text{PD,ref}}$. In other words, $t_{\text{PD,nor},j}$ is established for comparing the sample-to-sample difference of t_{PD} one another only from the perspective of the sample-to-sample variation of mobility excluding the other sample-to-sample differences, such as C_{OX} , C_{Load} , V_{MID} , V_{T} , and W/L .

By taking the Sample B as reference, the relation of $t_{\text{PD,nor},j}/t_{\text{PD,ref}} = 1/(\mu_j/\mu_{\text{ref}})$ was confirmed among μ_{IPD} , μ_{FE} , and μ_{avg} as shown in Fig. 5. Here, $t_{\text{PD,nor},j}$ and $t_{\text{PD,ref}}$ were taken from the sample-dependent t_{PD} measured in Table II, and also calculated using (11) and the parameters in Tables I and II. In addition, μ_j and μ_{ref} were taken from the mobilities measured in Table II.

Fig. 5 shows that among three kinds of mobilities, only μ_{IPD} obeys the relationship of $t_{\text{PD,nor},j}/t_{\text{PD,ref}} = 1/(\mu_j/\mu_{\text{ref}})$. It also suggests the μ_{avg} fails to quantify the link with carrier mobility and t_{PD} . We think the reason why the μ_{avg} fails to obey the relation of $\mu \propto 1/t_{\text{PD}}$ is that the carrier charge in subthreshold operation region affects the charging and discharging operations of IGZO TFT-based circuits. As it is well known, the μ_{avg} is based on the following premise. The TFT should be operating in the linear operation region, and it should be in above-threshold region. However, in an actual circuit, the t_{PD} is determined by the transition between the subthreshold and above-threshold regions. Such reasons support the need of alternative mobility metric that can reproduce the combination of subthreshold and above-threshold characteristics. Undoubtedly, combining the subthreshold and above-threshold operation regions can be efficiently accomplished by introducing the μ_{CB} , which takes Q_{free} and Q_{loc} into account in both the subthreshold and above-threshold regions.

From the viewpoint of combining the subthreshold and above-threshold characteristics, the subgap DOS is very important because it controls the position of Fermi level, i.e., the carrier density and distribution under a specific bias condition, in the subthreshold as well as the above-threshold

operation regions. Thus, we discovered the $\mu_{t_{PD}}$ is the best correlated to the circuit delay, and it can be extracted from the backbone of charge-based mobility along with our proposed parameter-extraction method and (1)–(10).

Therefore, the unknown $t_{PD,nor,j}$ can be estimated from the measured $t_{PD,ref}$, the experimentally extracted $\mu_{t_{PD,ref}}$ and $\mu_{t_{PD,j}}$ with our method. From our results, it is verified that the proposed $\mu_{t_{PD}}$ extraction method is suitable for predicting t_{PD} in high mobility IGZO TFT-based circuits, since predicting the t_{PD} using the mobility extracted from the I – V characteristic of TFT without measuring t_{PD} of the inverter is the main point we are focusing on.

As mentioned in Section IV, the conventional μ_{FE} extraction, i.e., $\mu_{FE} = g_m/[C_{OX}(W/L) \times V_{DS}]$ which is based on the assumption of V_{GS} -independent μ_{FE} during derivation of g_m in the linear region, may cause critical error in terms of the V_{GS} -dependence. However, it has not been significantly problematic in the low mobility amorphous silicon (a-Si) TFTs, since μ_{Band} itself is low and $Q_{loc} \gg Q_{free}$ due to the E_F -pinning by relatively high subgap DOS and thus, the V_{GS} -dependent $Q_{loc}(V_{GS})$ behavior is hard to be prominently observed in the conventional a-Si TFTs [15]. On the other hand, in cases of the high mobility amorphous oxide (e.g., a-IGZO) TFTs, Q_{free} becomes comparable with Q_{loc} and even $Q_{free}(V_{GS}) > Q_{loc}(V_{GS})$ becomes the case as V_{GS} increases, which means that the V_{GS} -dependence of μ_{FE} can be more complicated in a-IGZO TFT than that of a-Si TFT. Moreover, the V_{GS} -dependent $Q_{loc}(V_{GS})$ itself become also significant, since the E_F -pinning becomes extremely weak in a-IGZO in comparison with a-Si. In case of proposed $\mu_{t_{PD}}$, it is well correlated with the actual measurement value of the circuit t_{PD} because it is based on a concept reflecting the complicated V_{GS} -dependence of DOS-dependent $Q_{free}(V_{GS})$ and $Q_{loc}(V_{GS})$.

The mobility model has been preliminarily derived as a part of I – V modeling in [4]; however, the model became further improved by extending it either to subthreshold or to above-threshold regions, intensively investigating the experimental mobility extraction technique, and validating the usefulness of $\mu_{t_{PD}}$ with a special emphasis on its correlation with the t_{PD} measured in real inverters. In addition, employing the result of various structure and physical parameters in the three types of inverters indicates that the $\mu_{t_{PD}}$ would be universally used in assessing t_{PD} only from the I – V characteristics of a-IGZO TFTs, which implies that the mobility model we proposed can minimize the $t_{PD} \propto 1/\mu$ relation-aspect errors in real a-IGZO circuits.

VI. CONCLUSION

We proposed a practical method for extracting the circuit propagation delay-correlated mobility, i.e., $\mu_{t_{PD}}$, from the electrical characteristics of a-IGZO TFTs with the detailed procedure of parameter extracting. The proposed $\mu_{t_{PD}}$ was found to be best correlated with the relation of $t_{PD} \propto 1/\mu$ in IGZO TFT-based inverters, which had various geometrical and physical model parameters, other than various mobilities in the literature.

Our results suggest that a new method for evaluating mobility is indispensable for the codesign that can link the integration of IGZO TFT devices and their circuit applications. From this point of view, combining the already-existing concept of the charge-based mobility, $\mu_{CB} = \mu_{Band} \times Q_{free}/(Q_{free} + Q_{loc})$, and the proposed method, i.e., considering μ_{Band} , $Q_{free}(V_{GS})$, and $Q_{loc}(V_{GS})$ in both subthreshold and above-threshold regions and incorporating the extracted DOS, can be one of promising alternatives for the t_{PD} -correlated mobility.

Considering that the mobility of IGZO TFT is significantly affected by the subgap traps in IGZO active film, the proposed $\mu_{t_{PD}}$ extraction technique should be utilized as a useful mobility metric in assessing the performance of IGZO TFT-based circuitry based upon the device characteristic of an a-IGZO TFT as well as in efficiently quantifying the influence of the fabrication process on the performance of circuits consisting of amorphous oxide TFTs, including a-IGZO TFTs.

REFERENCES

- [1] J. Y. Kwon, "Bottom-gate gallium indium zinc oxide thin-film transistor array for high-resolution AMOLED display," *IEEE Electron Device Lett.*, vol. 29, no. 12, pp. 1309–1311, Dec. 2008.
- [2] H. Yin *et al.*, "High performance low voltage amorphous oxide TFT enhancement/depletion inverter through uni-/bi-layer channel hybrid integration," in *Proc. IEEE IEDM*, Dec. 2009, pp. 1–4.
- [3] B. Kim *et al.*, "Highly reliable depletion-mode a-IGZO TFT gate driver circuits for high-frequency display applications under light illumination," *IEEE Electron Device Lett.*, vol. 33, no. 4, pp. 528–530, Apr. 2012.
- [4] M. Bae *et al.*, "Analytical models for drain current and gate capacitance in amorphous InGaZnO thin-film transistors with effective carrier density," *IEEE Electron Device Lett.*, vol. 32, no. 11, pp. 1546–1548, Nov. 2011.
- [5] P. Servati, D. Striakhilev, and A. Nathan, "Above-threshold parameter extraction and modeling for amorphous silicon thin-film transistors," *IEEE Trans. Electron Devices*, vol. 50, no. 11, pp. 2227–2235, Nov. 2003.
- [6] M. Shur, M. Hack, and J. G. Shaw, "A new analytic model for amorphous silicon thin-film transistors," *J. Appl. Phys.*, vol. 66, no. 7, pp. 3371–3380, Oct. 1989.
- [7] T. Leroux, "Static and dynamic analysis of amorphous-silicon field-effect transistors," *Solid-State Electron.*, vol. 29, no. 1, pp. 47–58, Jan. 1986.
- [8] S. Lee *et al.*, "Trap-limited and percolation conduction mechanisms in amorphous oxide semiconductor thin film transistors," *Appl. Phys. Lett.*, vol. 98, no. 20, p. 203508, May 2011.
- [9] K. Nomura, T. Kamiya, H. Ohta, K. Ueda, M. Hirano, and H. Hosono, "Carrier transport in transparent oxide semiconductor with intrinsic structural randomness probed using single-crystalline InGaO₃(ZnO)₅ films," *Appl. Phys. Lett.*, vol. 85, no. 11, p. 1993, Sep. 2004.
- [10] J. Robertson, "Disorder and instability processes in amorphous conducting oxides," *Phys. Status Solidi B*, vol. 245, no. 6, pp. 1026–1032, Apr. 2008.
- [11] S. Lee, Y. W. Jeon, S. Kim, D. Kong, D. H. Kim, and D. M. Kim, "Comparative study of quasi-static and normal capacitance–voltage characteristics in amorphous indium-gallium-zinc-oxide thin film transistors," *Solid-State Electron.*, vol. 56, no. 1, pp. 95–99, 2011.
- [12] S. Lee *et al.*, "Extraction of subgap density of states in amorphous InGaZnO thin-film transistors by using multifrequency capacitance–voltage characteristics," *IEEE Electron Device Lett.*, vol. 31, no. 3, pp. 231–233, Mar. 2010.
- [13] R. L. Hoffman, "ZnO-channel thin-film transistors: Channel mobility," *J. Appl. Phys.*, vol. 95, no. 10, pp. 5813–5819, May 2004.
- [14] N. D. Arora, *MOSFET Models for VLSI Circuit Simulation: Theory and Practice*. New York, NY, USA: Springer-Verlag, 1993.
- [15] M. S. Shur, H. C. Slade, M. D. Jacunski, A. A. Owusu, and T. Ytterdal, "SPICE models for amorphous silicon and polysilicon thin film transistors," *J. Electrochem. Soc.*, vol. 144, no. 8, pp. 2833–2839, Aug. 1997.



Kyung Min Lee received the B.S. and M.S. degrees in electrical engineering from Kookmin University, Seoul, Korea, in 2013 and 2015, respectively.

He is currently with Samsung Electronics Company, Ltd., Seoul. His current research interests include oxide thin-film transistor devices and nanoCMOS devices.



Jaeman Jang received the B.S., M.S., and Ph.D. degrees in electrical engineering from Kookmin University, Seoul, Korea, in 2009, 2011, and 2015, respectively.

He is currently with the Research and Development Center, LG Display, Paju, Korea, as a Research Engineer. His current research interests include design, characterization, and modeling of oxide thin-film transistors and organic thin-film transistors.



Sung-Jin Choi received the M.S. and Ph.D. degrees in electrical engineering from the Korea Advanced Institute of Science and Technology, Daejeon, Korea, in 2012.

He is currently an Assistant Professor with the School of Electrical Engineering, Kookmin University, Seoul, Korea.



Dong Myong Kim (S'86–M'88) is currently a Professor with the School of Electrical Engineering, Kookmin University, Seoul, Korea. His current research interests include fabrication, characterization, and modeling of nanostructure silicon devices, III–V compound semiconductor devices, memories, and CMOS RF circuits.



Kyung Rok Kim (M'10) is currently an Associate Professor with the School of Electrical and Computer Engineering, Ulsan National Institute of Science and Technology, Ulsan, Korea. His current research interests include future CMOS and memory devices, neuromorphic devices, and terahertz plasma-wave devices.



Dae Hwan Kim (M'08–SM'12) received the B.S., M.S., and Ph.D. degrees in electrical engineering from Seoul National University, Seoul, Korea, in 1996, 1998, and 2002, respectively.

He is currently an Associate Professor with the School of Electrical Engineering, Kookmin University, Seoul, Korea. His current research interests include nanoCMOS, oxide and organic thin-film transistors, biosensors, and neuromorphic devices.